Carbohydrate Polymers 83 (2011) 1834–1842

Contents lists available at ScienceDirect

Carbohydrate Polymers

journal homepage: www.elsevier.com/locate/carbpol

Surface acetylation of cellulose nanocrystal and its reinforcing function in poly(lactic acid)

Ning Lin[a], Jin Huang[a,e,f,*], Peter R. Chang[b,**], Jiwen Feng[c], Jiahui Yu[d]

[a] College of Chemical Engineering, Wuhan University of Technology, Wuhan 430070, China
[b] Bioproducts and Bioprocesses National Science Program, Agriculture and Agri-Food Canada, 107 Science Place, Saskatoon, SK, S7N 0X2, Canada
[c] State Key Laboratory of Magnetic Resonance and Atomic and Molecular Physics, Wuhan Institute of Physics and Mathematics, Chinese Academy of Science, Wuhan 430071, China
[d] Interdisciplinary Science and Technology Institute for Advanced Study, East China Normal University, Shanghai 200062, China
[e] State Key Laboratory of Pulp and Paper Engineering, South China University of Technology, Guangzhou 510640, China
[f] Key Laboratory of Cellulose and Lignocellulosics Chemistry, Guangzhou Institute of Chemistry, Chinese Academy of Sciences, Guangzhou 510640, China

ARTICLE INFO

Article history:
Received 21 September 2010
Received in revised form 16 October 2010
Accepted 20 October 2010
Available online 27 October 2010

Keywords:
Cellulose nanocrystal
Acetylation
Poly(lactic acid)
Reinforcing

ABSTRACT

A novel and facile method for surface acetylation of cellulose nanocrystals (CN) was developed by reaction with acetic anhydride and hydroxyl groups on the surface of CN. The resultant acetylated cellulose nanocrystals (ACN) exhibited improved dispersion in various organic solvents and reduced polarity as compared with unmodified CN. These ACN were subsequently introduced into a poly(lactic acid) (PLA) polymeric matrix to produce fully biodegradable nanocomposites, which showed superior mechanical performance and thermal stability. This improvement was primarily attributed to uniform dispersion of the ACN and to strong interfacial adhesion between filler and matrix. This high performance and eco-friendly nanocomposite will expand the utilization of cellulose nanocrystals from renewable bioresources and the practical application of PLA-based plastic.

1. Introduction

It has been proposed that polysaccharides were the first biopolymers to have formed on Earth (Tolstoguzov, 2004). As one of the most important subgroups of polysaccharides, cellulose is a ubiquitous and abundant structural polymer found in plants and animals, and even in primeval organisms such as bacteria, fungi, algae and amoebas. Cellulose nanocrystals (CN) have attracted a great deal of interest in the nanocomposites field due to their appealing intrinsic properties including nanoscale dimensions, high surface area, unique morphology, low density, and mechanical strength, as well as the fact that they are readily available, renewable and biodegradable (Habibi, Lucia, & Rojas, 2010). Furthermore, abundant hydroxyl groups on the surface of CN are suitable for chemical modification including esterification, etherification, oxidation, silylation, and polymer grafting (Dufresne, 2010; Eichhorn et al., 2010). As such, numerous researchers have attempted to take advantage of these attributes. CN were first introduced as reinforcing nanofiller in poly(styrene-*co*-butyl acrylate)-based nanocomposites by Favier et al. (Favier et al., 1995). Since then, CN or modified CN have been used as fillers to enhance a wide range of synthetic polymeric matrices such as poly(oxyethylene) (Azizi Samir, Alloin, & Dufresne, 2005; Azizi Samir, Alloin, Sanchez, Kissi, & Dufresne, 2004; Azizi Samir, Chazeau, et al., 2005), polypropylene (Ljungberg, Cavaillé, & Heux, 2006), polyethylene (de Menezes, Siqueira, Curvelo, & Dufresne, 2009), poly(vinyl chloride) (Chazeau, Cavaillé, & Terech, 1999; Chazeau, Paillet, & Cavaillé, 1999; Chazeau, Cavaillé, & Perez, 2000), poly(vinyl alcohol) (Paralikar, Simonsen, & Lombardi, 2008), poly(vinyl acetate) (Garcia de Rodriguez, Thielemans, & Dufresne, 2006; Roohani et al., 2008); poly(β-hydroxyoctanoate) (Dubief, Samain, & Dufresne, 1999), poly(methylmethacrylate) (Liu, D., Zhong, Chang, Li, & Wu, 2010; Liu, H., Liu, Yao, & Wu, 2010), poly(lactic acid) (Bondeson & Oksman, 2007; Oksman, Mathew, Bondeson, & Kvien, 2006; Petersson, Kvien, & Oksman, 2007), poly(caprolactone) (Habibi & Dufresne, 2008; Habibi et al., 2008), poly(ethylene-*co*-vinyl acetate) (Chauve, Heux, Arouini, & Mazeau, 2005), poly(3-hydroxybutyrate-*co*-3-hydroxyvalerate) (Jiang, Morelius, Zhang, Wolcott, & Holbery, 2008; Ten, Turtle, Bahr, Jiang, & Wolcott, 2010), epoxide (Ruiz, Cavaillé, Dufresne, Gérard, & Graillat, 2000), cellulose acetate butyrate (Grunert & Winter, 2002; Petersson, Mathew, & Oksman, 2009), carboxymethyl cellulose (Choi & Simonsen, 2006), polyurethane (Marcovich, Auad, Bellesi, Nutt, & Aranguren, 2006), and waterborne polyurethane (Cao, Habibi, & Lucia, 2009).

* Corresponding author at: College of Chemical Engineering, Wuhan University of Technology, 122 Loushi Road, Wuhan 430070, China. Tel.: +86 27 63373510; fax: +86 27 87859019.
** Corresponding author.
E-mail addresses: huangjin@iccas.ac.cn (J. Huang), peter.chang@agr.gc.ca (P.R. Chang).

0144-8617/$ – see front matter © 2010 Elsevier Ltd. All rights reserved.
doi:10.1016/j.carbpol.2010.10.047

To realize their role in enhancing polymer composites, CN must be homogeneously dispersed in the polymeric matrix; however, due to their high surface area and hydrophilic nature, both intermolecular and intramolecular hydrogen bonding cause the nanocrystals to aggregate, resulting in inefficient compounding with most nonpolar thermoplastics (Azizi Samir, Alloin, et al., 2005; Azizi Samir, Chazeau, et al., 2005). Although some solvents, such as *N*,*N*-dimethylformamide (DMF) with N atom on the structure, can weaken the inter-chain bonding in cellulose to form a new hydrogen bond structure, such as O–H···N between the hydroxyl group on the cellulose and the N atom of the solvent molecules (Wu, Henriksson, Liu, & Berglund, 2007); these solvents (particularly organic solvents) were very limited in terms of practicality. To extend the applications for CN as nanofiller in composites, the surface properties of nanocrystals should be transformed to inhibit self-aggregation and improve dispersion and interfacial adhesion in various polymeric matrices. Concurrently, during CN modification the intrinsic structure of the nanocrystals, i.e. the original crystalline structure, should not be destroyed (Dufresne, 2006, 2008).

In this work, the surface of cellulose nanocrystals was chemically modified by acetic anhydride to provide acetylated cellulose nanocrystals (ACN). To best of our knowledge, this reaction has not been exploited for the modification of CN and has definitely not been compounded in PLA-based composites. It is hypothesized that acetylation will improve the dispersion of CN in organic solvents. It is further hypothesized that the addition of ACN filler will promote miscibility and interfacial adhesion with the polyester matrix, ultimately enhancing mechanical performance and thermal stability of the resultant composites. In this study, successful acetylation was confirmed by the results of Fourier transform infrared spectroscopy (FTIR), and solid state ^{13}C cross polarization-magic angle spinning (CP-MAS) NMR spectra (^{13}C CP-MAS NMR). Maintenance of the crystalline structure of ACN was revealed by X-ray diffraction (XRD). The morphologies of both modified and unmodified nanocrystals were observed by means of transmission electron microscopy (TEM). Wettability experiments and contact angle measurements were used to investigate changes in solubility and surface properties of ACN. In addition, PLA/ACN nanocomposites were characterized using tensile measurements, dynamic mechanical analysis (DMA), differential scanning calorimetry (DSC), XRD, and scanning electron microscopy (SEM). Finally, the roles of nanocrystals and interactions between the filler and matrix were discussed.

2. Materials and methods

2.1. Materials

Commercial poly(lactic acid) (PLA) pellets with the number-average molar weight and polydispersity of 8.1×10^4 Da and 1.80, respectively, were purchased from Shenzhen Bright China Industrial Co., Ltd. (Shenzhen, China). The linter was kindly supplied by Hubei Chemical Fiber Group Co., Ltd. (Xiangfan, Hubei, China). Acetic anhydride was purchased from Xilong Chemical Industry Inc. Co. Ltd. (Shantou, China). Pyridine was dried and purified according to standard procedures. Sulfuric acid (H_2SO_4), dichloromethane (CH_2Cl_2), acetone (C_3H_6O) and other analytical-grade reagents were purchased from Shanghai Sinopharm Chemical Reagent Co., Ltd. (Shanghai, China) and used without further purification.

2.2. Extraction of cellulose nanocrystals

Cellulose nanocrystals (CN) were prepared by H_2SO_4 hydrolysis of native linter using the following method (Lin, Chen, Huang, Dufresne, & Chang, 2009): The linter (20.0 g) was dispersed in 175 mL of 30% (v/v) aqueous H_2SO_4 and stirred constantly at 100 rpm for 6 h at 60 °C. Disordered or paracrystalline regions of cellulose were preferentially hydrolyzed, whereas crystalline regions that have a higher resistance to acid attack remained intact (Ruiz et al., 2000). The resultant suspension was washed by successive centrifugation with distilled water until approximate neutrality was achieved. A small amount of ammonia (0.5 wt%) was added to remove the sulfate groups from the CN surface. The suspension was then dialyzed overnight against distilled water and finally, a loose powder was obtained by freeze–drying the CN.

2.3. Acetylation of cellulose nanocrystals

Acetylation was performed with constant stirring under a nitrogen atmosphere in a three-necked round-bottomed flask equipped with a condenser. A suspension of 1.0 g cellulose nanocrystals and 20 mL anhydrous pyridine was dispersed by 15 min of ultrasonic treatment and then added to the flask. Chemical modification was started by dropwise addition of a solution of 5 mL acetic anhydride in anhydrous pyridine to the CN suspension. The reaction mixture was kept at 80 °C and stirred at 400 rpm for 5 h. After the reaction, the product was isolated by precipitation in 1.0 L of water and washed three times with water; it was then purified by washing with a solution of acetone/water which eliminated all non-bonded chemicals (i.e., unreacted compounds and reaction by-products). Finally, the acetylated cellulose nanocrystals, coded as ACN, were oven-dried under vacuum at 60 °C for 12 h.

2.4. Preparation of the PLA nanocomposites filled with ACN

The desired amount of ACN was added along with 2.0 g of PLA into CH_2Cl_2 with mechanical stirring to produce a mixture. The mixture was then conditioned overnight to eliminate bubbles and was then cast into a Teflon mold. The CH_2Cl_2 was allowed to evaporate off at ambient temperature (ca. 25 °C) for 24 h. Finally, the solidified films, with a thickness of about 0.2 mm, were vacuum-dried overnight, and then kept in a desiccator containing silica gel. The resultant nanocomposite sheets were coded as PLA/ACN-1, PLA/ACN-2, PLA/ACN-4, PLA/ACN-6, PLA/ACN-8 and PLA/ACN-10; the Arabic numerals represented the theoretical ACN content in the nanocomposites. A neat PLA film was also prepared according to the aforementioned process without the addition of ACN, and it was coded as PLA-F.

2.5. Characterization

2.5.1. Fourier transform infrared (FT-IR) spectroscopy

FTIR spectra of the powdered CN and ACN, as well as all the nanocomposite sheets, were recoded on an FTIR 5700 spectrometer (Nicolet, Madison, WI). The powders were measured using a KBr-pellet method in the range of 4000–400 cm^{-1}, and the nanocomposite sheets were scanned in the range of 4000–700 cm^{-1} using Smart OMNT reflection accessories.

2.5.2. X-ray diffraction analysis (XRD)

X-ray diffraction (XRD) measurements were performed on dry powders of CN and ACN, as well as on all the nanocomposite sheets, at ambient temperature on a D/max-2500 X-ray diffractometer (Rigaku Denki, Tokyo, Japan) with Cu $K\alpha_1$ radiation ($\lambda = 0.154$ nm) in a range of $2\theta = 3–70^\circ$ using a fixed time mode with a step interval of 0.02°.

2.5.3. ^{13}C CP-MAS NMR Spectroscopy

Solid state ^{13}C cross polarization-magic angle spinning (CP-MAS) NMR spectra of CN and ACN were recorded at ambient temperature on a Varian Infinity-Plus 300 NMR spectrometer, using

Table 1
Contact angle (θ), nonpolar component (γ_S^d), polar component (γ_S^p) and surface energy (γ_S) values of unmodified (CN) and acetylated cellulose nanocrystals (ACN).

Sample	θ (°)			γ_S^d [a] (mJ m^{-2})	γ_S^p (mJ m^{-2})	γ_S (mJ m^{-2})
	Water	Diiodomethane	Glycerol			
CN	44.7	19.0	21.3	39.4	21.3	60.7
ACN	78.0	12.1	49.7	47.2	2.8	50.0

[a] The surface tensions of three standard liquids were taken from the literatures (Adão et al., 1999; Michalski et al., 1998) and are as follow: the γ_L, γ_L^d and values of water are 72.8, 21.8 and 51.0 mJ m^{-2}, respectively; the γ_L, γ_L^d and γ_L^p values of diiodomethane are 50.8, 49.5 and 1.3 mJ m^{-2}, respectively; the γ_L, γ_L^d and γ_L^p values of water are 37.0, 26.4 and 63.4 mJ m^{-2}, respectively.

a MAS rate of 6 kHz, at a frequency of 75.5 MHz for ^{13}C NMR. Samples were packed in MAS 4-mm-diameter zirconia rotors. All spectra were run for 3 h (3000 scans).

2.5.4. Contact angle measurements

Contact angle measurements were performed at ambient temperature using a dynamic drop tensiometer (DSA10, KRUSS, Germany). The contact angle and drop volume were monitored as a function of time using WINDROP software. Three different liquids, with different dispersive and polar surface tensions, were used to determine the surface energy of CN. The drop volume was ca. 5 μL. The powdered CN was compacted under a pressure of 20 MPa with a KBr press to obtain samples with smooth surfaces. Contact angle measurements were carried out on CN before and after surface modification.

The Owens–Wendt approach was used to relate the dispersive and polar contributions of the surface energies of the cellulose nanocrystal samples to the dispersive and polar contributions of the surface tension of the liquids used, and to their equilibrium contact angle with the cellulose nanocrystals surface (where the work of adhesion is replaced by the Young equation):

$$\gamma_L(1+\cos\theta) = 2\sqrt{\gamma_L^d\gamma_S^d} + 2\sqrt{\gamma_L^p\gamma_S^p}$$

The variables of γ, γ^d, and γ^p represented the total, dispersive, and polar surface energies, respectively. Subscripts L and S refer to the liquid drop (L) and the solid surface (S), and θ denote the contact angle between the solid substrate and the liquid drop. The liquid surface tensions were taken from the literatures (Adão, Saramago, & Fernandes, 1999; Michalski, Hardy, & Saramago, 1998) and are listed in the Footnotes for Table 1, respectively.

2.5.5. Transmission electron microscopy (TEM)

TEM observations were carried out on an H-7000FA electron microscope (Hitachi, Tokyo, Japan) at 75 kV. Very small amounts of powdered CN and ACN were dispersed separately in distilled water, and then negatively stained with a 2% (w/v) ethanol solution of uranyl acetate.

2.5.6. Tensile measurements

The mechanical parameters, including tensile strength (σ_b), elongation at break (ε_b), and Young's modulus (E), of all the nanocomposite sheets were measured on a CMT6503 universal testing machine (SANS, Shenzhen, China) with a tensile rate of 10 mm min^{-1} according to ISO 527-3:1995(E). The testing sheets were cut into strips with a width of 10 mm and a distance of 30 mm between testing marks. The testing strips were kept at 35% humidity for 7 days before measurement. A mean value of five replicates from each sheet was taken.

2.5.7. Differential scanning calorimetry analysis (DSC)

DSC analysis was performed on a DSC-Q200 instrument (TA Instruments, New Castle, Delaware, United States) under a nitrogen atmosphere at a heating or cooling rate of 20 °C min^{-1}. About 2 mg powdered CN and ACN were placed in hermetically sealed DSC crimp pans, which were tested over a range of −100 to 350 °C. All the nanocomposites were scanned over a range of −100 to 200 °C after a pretreatment of heating from 20 to 100 °C and then cooling to −100 °C to eliminate thermal history.

2.5.8. Dynamic mechanical analysis (DMA)

DMA was performed on a DMA 242C dynamic mechanical analyzer (Netzsch, Hanau, Germany) with a dual cantilever device at a frequency of 3 Hz. The temperature range was from −100 to 200 °C with a heating rate of 3 °C/min. The dimensions of the test specimens (with a thickness of ca. 0.20 mm) were 30 mm × 10 mm.

2.5.9. Scanning electron microscopy (SEM)

SEM observations were carried out on an X-650 scanning electron microscope (Hitachi, Tokyo, Japan). All the nanocomposite sheets were frozen in liquid nitrogen and then immediately snapped. The fracture surfaces of the sheets were sputtered with gold and then observed and photographed.

3. Results and discussion

3.1. Acetylation of cellulose nanocrystals

3.1.1. Chemical modification of CN

The expected acetylation of cellulose nanocrystals is shown by the chemical reaction scheme in Fig. 1A. Using FTIR spectroscopy, this reaction was characterized by the appearance of a new peak in the carbonyl area around 1746 cm^{-1} that was associated with the formed ester group, shown in Fig. 1C. A new absorption band at 1240 cm^{-1} was assigned to the carbonyl C–O stretch vibration. Furthermore, the intensity of peaks located at 3342 cm^{-1}, assigned to O–H stretching of the cellulose nanocrystal component, decreased after the acetic anhydride chemical modification; successful acetylation of ACN was thereby indicated.

Acetylated cellulose nanocrystals were further characterized by ^{13}C CP-MAS NMR spectroscopy (Fig. 1D). As in a previous report (Attala, Gast, Sindorf, Bartuska, & Maciel, 1980), carbons of the original CN were assigned as follows: C1 (105 ppm), C4 crystalline (89 ppm), C4 amorphous (84 ppm), C2/C3/C5 (72 and 75 ppm), C6 crystalline (65 ppm), and C6 amorphous (63 ppm). With acetylation there were two chemical shifts located at 172 and 20 ppm assigned, respectively, to Ca (–C=O) and Cb (–CH_3) (shown in Fig. 1A) of the acetyl group on ACN, which confirmed the successful modification of CN.

3.1.2. Morphologies and crystalline properties of CN and ACN

TEM was used to investigate morphological changes of the cellulose nanocrystals associated with the surface acetylation. The ungrafted CN had a rodlike morphology with a length of 200–300 nm and a diameter of 10–20 nm, as shown in the TEM image in Fig. 1B, as was also found in our previous report (Lin et al., 2009). After acetylation of CN, it seemed that the rodlike shape (shown in Fig. 1B) was preserved, but its size was slightly decreased. In addition, the outline of the ACN was blurry, which may have resulted from partial solubilization of the cellulose molecules dur-

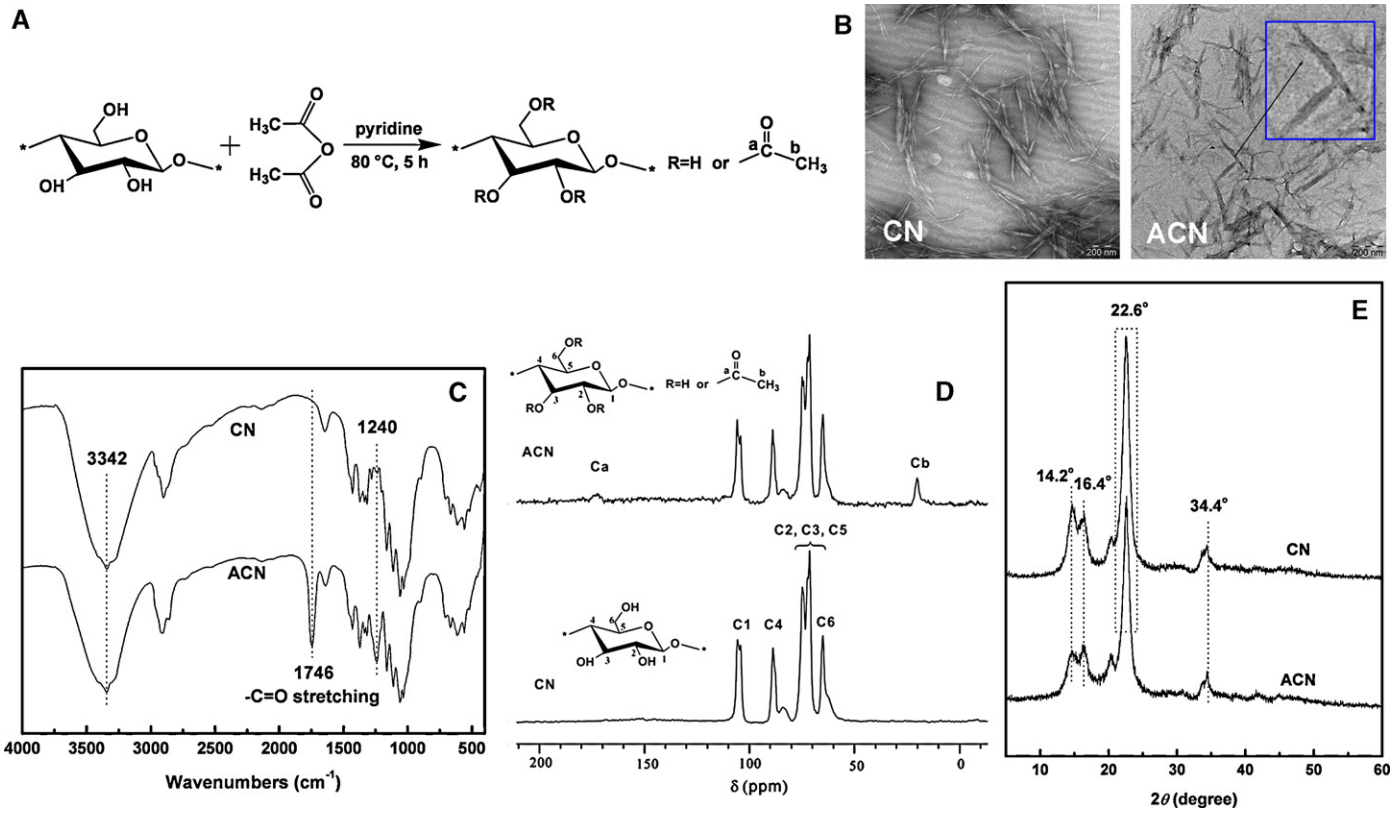

Fig. 1. (A) Acetylation of CN by the chemical reaction between cellulose hydroxyl groups and acetic anhydride; (B) TEM images of unmodified CN and ACN; (C) FTIR spectra of unmodified CN and ACN; (D) ^{13}C CP-MAS NMR spectra of unmodified CN and ACN; (E) XRD patterns of CN and ACN.

ing acetylation. The intrinsic morphology and structure of the nanocrystals were however preserved.

The impact of chemical modification on the crystallite structure of the cellulose nanocrystals was further investigated using XRD analysis. The diffraction patterns for unmodified CN and ACN are presented in Fig. 1E. The diffraction peaks of the 2θ angles at about 22.6°, 16.4°, and 34.4° were assigned to the typical reflection planes of cellulose I, 0 0 2, 1 0 1, and 0 4 0 (Liu, D., et al., 2010; Liu, H., et al., 2010), respectively. Although the intensities of the 0 0 2 and 1 0 1 planes decreased slightly in ACN, crystalline characteristics similar to CN were still clearly present, indicating that the original inner crystalline structure of the nanocrystals was maintained. This change is consistent with the TEM results.

3.1.3. Wettability and polarity of CN and ACN

As mentioned above, CN without surface modification have intrinsically strong interactions and have been reported as notoriously difficult to disperse. The acetylation of CN markedly improved their dispersion in both water and organic solvents. CN and ACN were added at 2 wt% into six different solvents including water, dichloromethane, acetone, toluene, tetrahydrofuran (THF) and DMF. The suspensions of acetylated nanocrystals showed outstanding dispersion and stability in all the solvents (as shown in Figure S1 in the section of Supplementary Data); the unmodified CN was inclined to self-aggregation and sedimented quickly to the bottom of the suspensions. The good dispersion of ACN in the various solvents may be attributed to the weakening of intra- and intermolecular hydrogen bonding due to modification of the hydroxyl groups on the surface of CN.

The transformation of the surface characteristics of CN and ACN was further confirmed by the results of the contact angle measurements. Table 1 summarizes the equilibrium contact angle for water, diiodomethane and glycerol on CN and ACN. The dependencies of contact angle, volume, and diameter of one drop of water upon time were traced respectively (as shown in Figure S2 in the section of Supplementary Data). Contact angle values and volumes of the drop on ACN decreased slightly and equably with time due to the spreading action, whereas the diameters of the drop increased slightly. On the contrary, the volumes and diameters of the drop on CN varied unsteadily with time, which may have resulted from swelling of the hydrophilic CN. The different performances of the change in dynamic contact angle on CN and ACN corroborate the occurrence of chemical modification. Photographs of water drops deposited on both unmodified CN and ACN surfaces (as shown in Figure S2 in the section of Supplementary Data) illustrate that water had a higher affinity for the surface of CN than ACN. Transformation of surface properties can also be deduced from the data in Table 1. The –OH rich CN surface was more capable of establishing hydrogen bonding with water and consequently resulted in lower initial contact angle value. This is consistent with reported literature (Fabbri, Champon, Castellano, Belgacem, & Gandini, 2004; Zini, Scandola, & Gatenholm, 2003). The ACN had a sharp increase in θ_{water} from 44.7° to 78.0°, and a decrease in $\theta_{diiodomethane}$ from 19.0° to 12.1° which indicated that chemical modification had induced dramatic changes in surface polarity of the cellulose nanocrystals. All the qualitative features were also observed when a drop of diiodomethane, a nonpolar liquid, was deposited on the same substrates. These observations were determined according to the Owens–Wendt approach, by the values of the polar and dispersive contributions to the surface energy, as given in Table 1. With the introduction of nonpolar groups to the surface of CN, the dispersive component evidently did not change, whereas the polar one decreased considerably. The polar component (γ_S^p) in cellulose nanocrystals decreased from 21.3 to 2.8 mJ m^{-2} and the total surface energy (γ_S) also decreased, from 60.7 to 50.0 mJ m^{-2}, which can be attributed to the substitution of hydrophilic –OH by acetyl

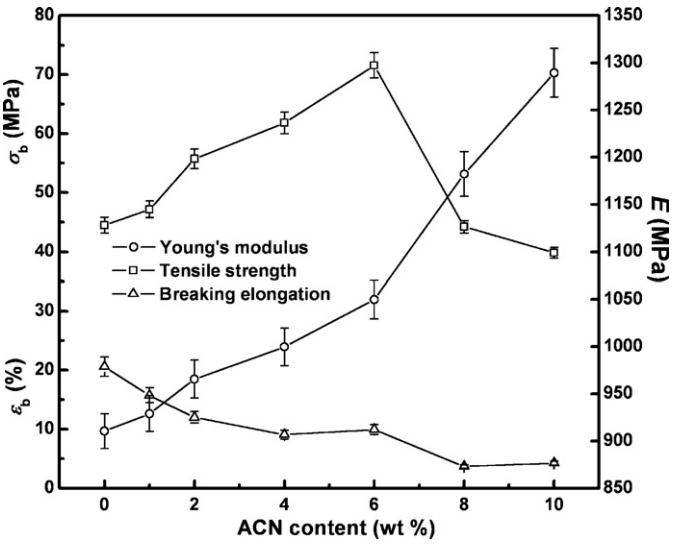

Fig. 2. Effect of the ACN content on σ_b, ε_b, and E for PLA/ACN nanocomposites as well as the neat PLA-F sheet.

groups and to the formation of intramolecular hydrogen bonding of the carbonyl groups. It should be pointed out that with the acetylation modification, transformation of the surface properties will improve the dispersion and interfacial adhesion of ACN in non-polar polymeric matrices, such as PLA and natural rubber, and ultimately tailor the performance of nanocomposites.

3.1.4. Thermal properties of CN and ACN

A change in thermal properties after chemical modification of cellulose nanocrystals was confirmed by DSC analysis (as shown in Figure S3 in the section of Supplementary Data). As previously reported, cellulose undergoes degradation between 200 and 300 °C (Wang, Ding, & Cheng, 2007; Xiao, Sun, & Sun, 2001). The decomposition temperature of ACN was ca. 15 °C higher than that of unmodified CN, which can be attributed to the replacement of surface hydroxyl groups with the more stable acetyl groups. This proved that acetylation markedly elevated the thermal stability of the original cellulose nanocrystals, an advantage for the improvement of thermal performance of the nanocomposites. It should be pointed out that the close decomposition temperatures of ACN and CN indicated that the chemical modification did not destroy the crystalline structure of the original CN, which was in agreement with the results of XRD.

3.2. Structure and properties of PLA/ACN nanocomposites

3.2.1. Mechanical properties of nanocomposites

Acetylated cellulose nanocrystals were incorporated into a PLA matrix, and Fig. 2 shows the effects of the ACN content on the mechanical parameters of the PLA/ACN nanocomposites including tensile strength (σ_b), elongation at break (ε_b), and Young's modulus (E). The σ_b of the nanocomposites increased gradually with an increase in the ACN content, up to the 6 wt% load level after which it decreased. In this case, the σ_b of the PLA/ACN-6 sheet reached a maximum value of 71.6 MPa, a 61.3% increase over the σ_b of the neat PLA-F sheet (44.4 MPa). All the PLA/ACN nanocomposites exhibited dramatically increased E values, and the nanocomposite with the highest loading level, PLA/ACN-10, had the maximum E value of 1289.5 MPa, which was about 1.5-fold greater than that of the neat PLA-F sheet. Meanwhile, the effect of changes in the ACN content on ε_b was just the opposite of that on E, and was attributed to the presence of rigid nanocrystals. The prominent improvements observed in the ACN-filled PLA system may be ascribed to the uniform distribution of ACN in the PLA matrix, and to the strong interfacial adhesion between filler and matrix. It was believed that with the addition of an appropriate amount of nanofiller (such as 6 wt%), acetylation of the nanocrystals' surface would inhibit self-aggregation and promote the dispersion of ACN. This would then serve as the stress–concentration point in the PLA matrix and contribute to the reinforcement of σ_b. When excess nanofiller was added, such as in PLA/ACN-8 and PLA/ACN-10, a rigid network formed among the nanocrystals in the composites, which greatly facilitated the enhancement of modulus; at the same time, the appearance of the rigid network and self-aggregation may have slightly damaged the original PLA polymer structure resulting in a decrease in the strength and elongation of these two composites. The prominent enhancement of strength as well as modulus, due to the addition of rigid ACN, could contribute to extended applications for PLA-based plastics.

3.2.2. Structural changes of nanocomposites

The XRD patterns for the PLA/ACN nanocomposites and the neat PLA-F sheet are depicted in Fig. 3A. Neat PLA was mainly comprised of the amorphous polymer structure, and the crystalline characteristic was ambiguous. Conversely, the ACN as nanofiller still maintained a highly crystalline characteristic. With an increase in loading level, the crystalline property of the cellulose nanocrystals exhibited two distinct diffraction peaks located at about 16.4° and 22.6° of 2θ. In particular, when enough ACN was introduced, as in PLA/ACN-8 and PLA/ACN-10, the presence of ACN, and even self-aggregated ACN, made the crystalline character assigned to the cellulose nanocrystals in the nanocomposite system more clear and definite.

Fig. 3B shows the full ATR-FTIR spectra of the PLA/ACN nanocomposites and the neat PLA-F. All the PLA-based composites showed a peak, characteristic of an ester group, located at ca. 1752 cm^{-1}. The nanofiller loading levels and the interactions between filler and matrix affected the distribution of –C=O in the ordered and amorphous regions of the nanocomposites. Curve-fitting was used to divide the spectra of all the PLA-based nanocomposites and the neat PLA-F (as shown in the legend of Fig. 3B) from 1650 cm^{-1} to 1850 cm^{-1} into three peaks, i.e. Peak I located at about 1774 cm^{-1} assigned to free –C=O; Peak II located at about 1753 cm^{-1} assigned to –C=O in the amorphous region; and Peak III located at about 1736 cm^{-1} assigned to –C=O in the ordered domain. Table 2 summarizes the detailed locations and fractions of Peaks I, II and III for all the samples. As shown by the XRD results, amorphous and free –C=O components were in the majority in neat PLA. With the introduction of low loading levels of ACN, such as 1 wt% and 2 wt%, uniform dispersion of rigid nanocrystals in the matrix inhibited the motion of polymer chains, and resulted in a decrease of –C=O in the amorphous fraction. The addition of more ACN, such as 4 wt% and 6 wt%, induced disorder in the system. Although the rigid nanocrystals still restricted the motion of free –C=O, the filler nanophase greatly affected the existence of –C=O in the ordered domain, and gradually decreased its fraction in the system. With the incorporation of superfluous nanofillers, clusters appeared due to self-aggregation of the ACN, and hence reduced the filler's effective active surface area available for interaction with the PLA matrix. This strongly restricted the motion of –C=O in both the free domain and the amorphous region, and ultimately resulted in an increase in the –C=O fraction of the ordered domain.

3.2.3. Thermal properties of nanocomposites

DSC and DMA were used to further understand the interactions between ACN and the PLA matrix, as well as structural changes or crystalline properties of the PLA matrix and the distribution of ACN, through the observation of variances in the domain-scale glass transition, the melting transition, and the molecular-level

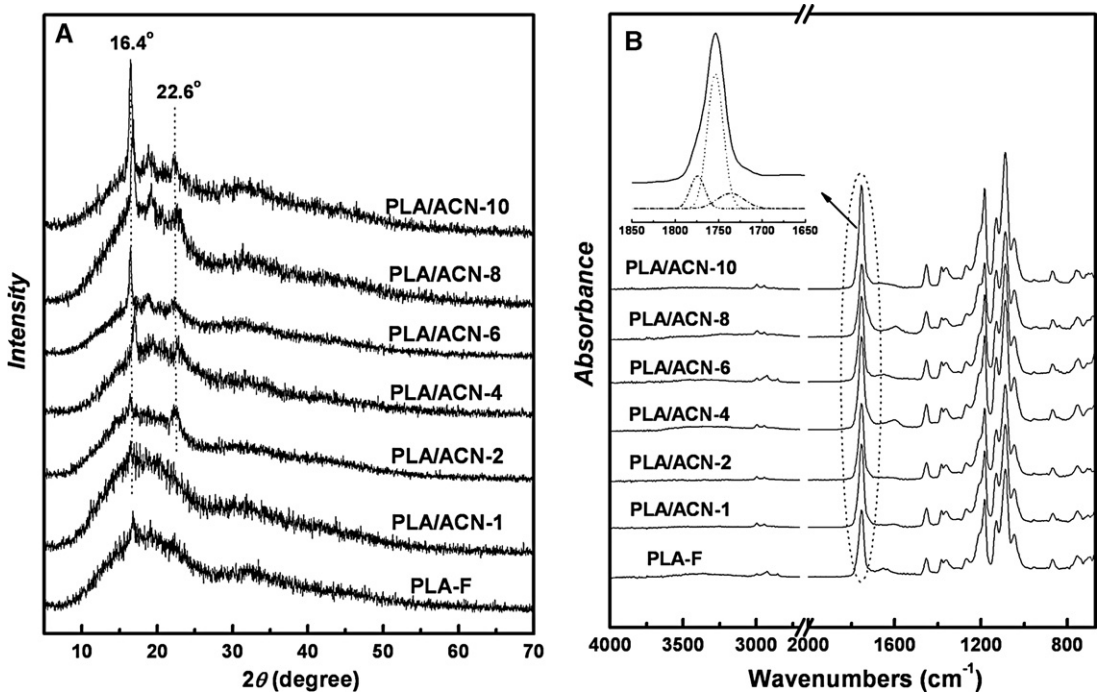

Fig. 3. (A) XRD patterns of PLA/ACN nanocomposites with various ACN contents, as well as the neat PLA-F sheet; (B) full ATR-FTIR spectra of PLA/ACN nanocomposites with various ACN contents and neat PLA-F sheet, as well as the curve-fitted FTIR spectra of PLA/ACN-10 in the range of 1600–1800 cm^{-1} for reference. (–– Experimental curve;.. -.. free –C=O;.... –C=O in amorphous region; -.-. –C=O in ordered domain).

α-relaxation assigned to the PLA component. DSC thermograms and data for the glass transition temperature at midpoint ($T_{g,mid}$), heat-capacity increment (ΔC_p), melting temperature (T_m), heat of fusion (ΔH_m), and degree of crystallinity within the PLA fraction (χ_c) of the nanocomposites are summarized in Table 3 (as shown in Figure S4 in the section of Supplementary Data). When the ACN content was less than 2 wt%, the rigid nanocrystals dispersed homogeneously in the PLA matrix, and inhibited the motion of components in the amorphous and free domains with the newly formed interactions between nanofiller and matrix. This restriction caused a higher energy requirement for the transformation of thermal behaviour of nanocomposites, ultimately resulting in an increase in $T_{g,mid}$ and ΔC_p. Meanwhile, at these low loading levels, due to the nucleation of nanocrystals, the crystallinity of the composites was elevated. Although the nanofillers still dispersed well in the matrix and formed a strong interfacial adhesion with the matrix with the introduction of 4 wt% and 6 wt% ACN, the presence of ACN affected the interactions between the crystalline and amorphous

Table 2
Location and fraction of curve-fitting peaks for –C=O absorption in the FTIR spectra of the PLA/ACN nanocomposites.

Sample	Peak I[a]		Peak II		Peak III	
	Location (cm^{-1})	Fraction (%)	Location (cm^{-1})	Fraction (%)	Location (cm^{-1})	Fraction (%)
PLA-F	1774.6	14.2	1753.6	74.7	1736.9	11.1
PLA/ACN-1	1774.0	15.0	1753.3	67.8	1736.2	17.2
PLA/ACN-2	1774.0	16.3	1753.3	65.8	1736.7	17.9
PLA/ACN-4	1774.0	13.2	1753.0	70.4	1736.8	16.4
PLA/ACN-6	1774.8	13.9	1753.3	71.2	1736.5	14.9
PLA/ACN-8	1774.0	12.3	1753.8	69.9	1736.5	17.8
PLA/ACN-10	1774.5	9.8	1752.7	68.3	1736.4	21.9

[a] Peak I: free –C=O; peak II: –C=O in amorphous region; peak III: –C=O in ordered domain.

Table 3
DSC and DMA data of the PLA/ACN nanocomposites as well as the neat PLA-F sheet.

Sample	DSC data					DMA data					
	$T_{g,mid}$ (°C)	ΔC_p ($J\,g^{-1}\,K^{-1}$)	T_m (°C)	ΔH_m ($J\,g^{-1}$)	χ_c[a] (%)	$T_{\alpha,onset}$ (°C)	log E'_{onset} (MPa)	$T_{\alpha1,max}$ (°C)	$H_{loss\text{-}peak,1}$	$T_{\alpha2,max}$ (°C)	$H_{loss\text{-}peak,2}$
PLA-F	43.0	0.39	145.2	18.7	20.1	38.3	3.35	47.1	0.32	65.1	0.44
PLA/ACN-1	44.9	0.40	146.0	24.1	26.2	45.1	3.32	48.0	0.29	65.1	0.71
PLA/ACN-2	45.3	0.42	146.1	25.3	27.8	36.8	3.40	45.3	0.29	65.1	0.37
PLA/ACN-4	40.5	0.34	146.3	23.8	26.7	36.9	3.31	54.3	0.26	64.1	0.30
PLA/ACN-6	41.5	0.35	146.9	23.6	27.0	37.5	3.35	55.2	0.31	63.9	0.31
PLA/ACN-8	42.3	0.39	147.2	25.5	29.8	39.9	3.40	49.2	0.35	65.8	0.39
PLA/ACN-10	49.7	0.44	145.4	27.2	32.5	44.6	3.42	48.1	0.20	66.2	0.47

[a] $\chi_c = \Delta H_m/\omega\Delta H_m^\circ$, where $\Delta H_m^\circ = 93.0\,J\,g^{-1}$, the heat of fusion 100% crystalline PLA (Martin & Avérous, 2001), and ω is the weight fraction of the polymeric matrix material in the final product.

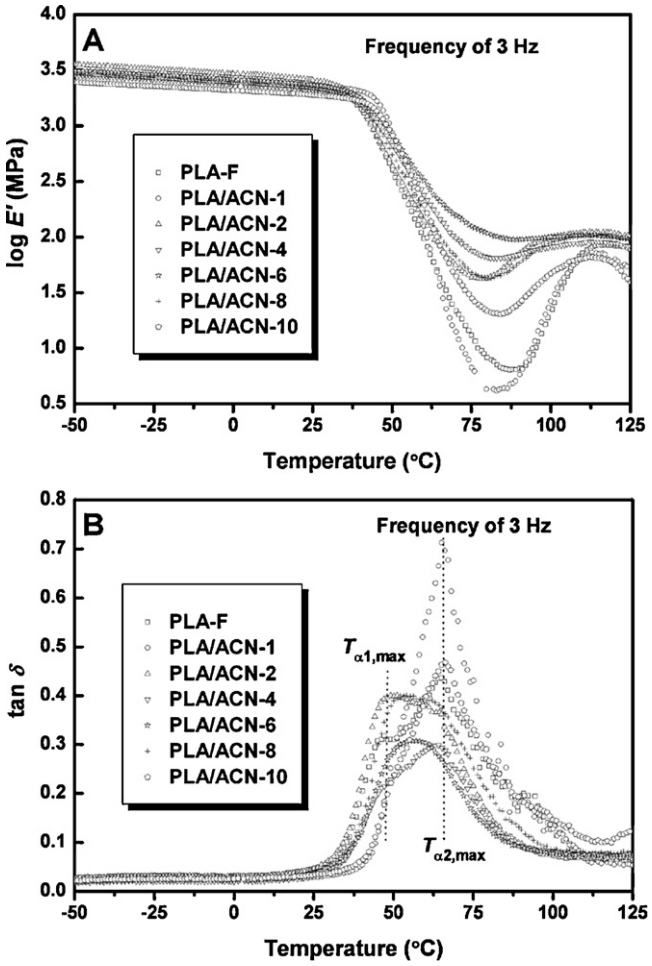

Fig. 4. DMA thermograms of the log E'-temperature curve (A) and tan δ–temperature curve (B) for PLA/ACN nanocomposites with various ACN contents and the neat PLA-F for reference.

structures resulting in decreased $T_{g,mid}$, ΔC_p and χ_c. However, the addition of superfluous ACN caused self-aggregation of nanofillers and again restrained the motion of the amorphous domain, and induced an increase in $T_{g,mid}$ and ΔC_p. In addition, large numbers of nanocrystals resulted in the dominance of the nucleation function in the change of crystalline properties and elevated the crystallinity of the composites.

Logarithmic curves of the storage modulus versus temperature (A) and the loss factor versus temperature (B) from DMA are shown in Fig. 4. The associated α-relaxation (corresponding to the glass transition), logarithm of storage modulus versus temperature, and loss factor versus temperature from DMA are summarized in Table 3. There was a marked drop in the storage modulus (E') of PLA-based nanocomposites at around 65–80 °C, as also found in a previous report (Martin & Avérous, 2001), that was attributed to the glass transition effects of the PLA component. It was interesting to note that there were two relaxation temperatures at the loss peak ($T_{\alpha,max}$), located at about 50 °C and 65 °C in the tan δ–temperature curves. The first temperature of $T_{\alpha 1,max}$ was assigned to the true relaxation temperature of the amorphous PLA component, whereas the second temperature of $T_{\alpha 2,max}$ was assigned to the relaxation temperature of amorphous PLA component adjacent with the crystalline PLA domains. The change tendency of $T_{\alpha 1,max}$ was in agreement with the results of DSC, namely that the relaxation temperature firstly increased to 55.2 °C of PLA/ACN-6 nanocomposite, and then gradually decreased with the increase of the ACN loading-level. The increase of the relaxation temperature of nanocomposites indicated that the addition of a certain ACN nanoparticles might inhibit the motion of the PLA segments in amorphous region.

3.2.4. Fracture morphologies of nanocomposites

Fig. 5 shows SEM images of the fracture morphologies of the PLA/ACN nanocomposites. The neat PLA-F sheet (Fig. 5A) presented a striated and smooth fractured surface. When the ACN loading level was lower than 2 wt % the modified nanocrystals dispersed homogeneously in the PLA matrix, as shown by the white dot in Fig. 5B and C. With the addition of 4 wt % and 6 wt % ACN (Fig. 5D and E), the nanocomposite fracture morphologies exhibited slightly coarse surfaces and maintained a striation similar to that of the neat PLA-F sheet. This indicated that when ACN appeared in the increased contents, they still exhibited good miscibility with matrix. Meanwhile, the introduction of ACN at these loading levels did not destroy the original structure of the PLA component. However, with a continuous increase in the loading level of ACN (higher than 8 wt %), some large conglomerations emerged and the composites showed a relatively brittle characteristic, shown in Fig. 5F

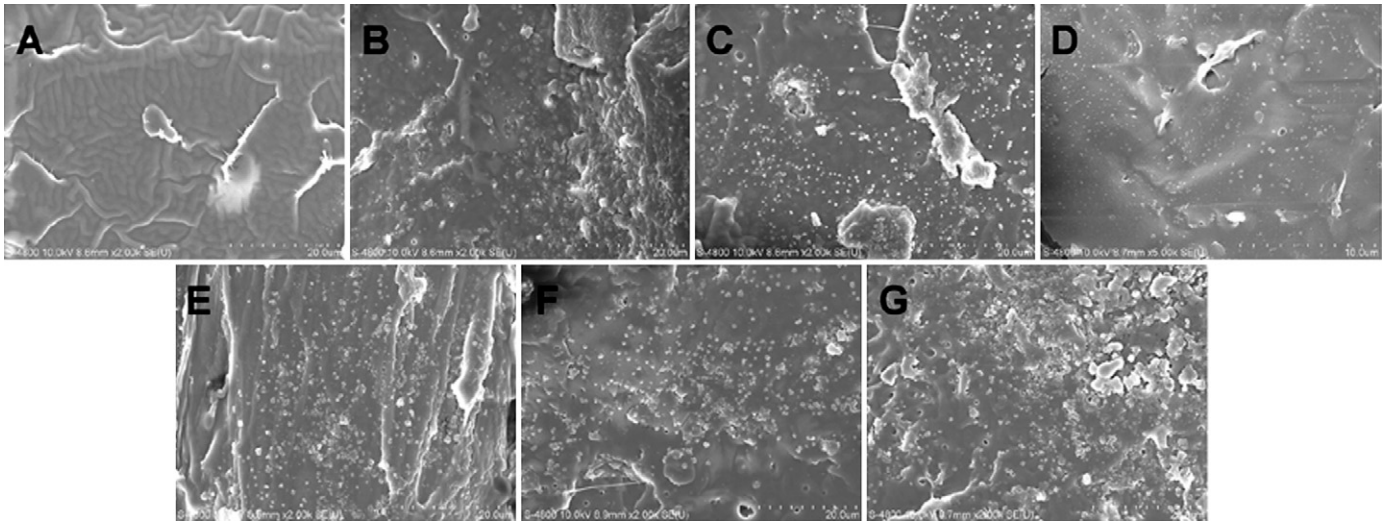

Fig. 5. SEM images of the fracture surfaces of the nanocomposites PLA/ACN-1 (B), PLA/ACN-2 (C), PLA/ACN-4 (D), PLA/ACN-6 (E), PLA/ACN-8 (F), PLA/ACN-10 (G) as well as neat PLA-F (A) for reference.

and G, which was attributed to self-aggregation of the superfluous nanofiller.

4. Conclusions

The crystalline structure of cellulose nanocrystals was maintained after modification with acetic anhydride. With the substitution of hydroxyl groups by acetyl groups on the CN surface, acetylated cellulose nanocrystals exhibited improved dispersion in six common solvents, a decrease in surface polarity, and a higher decomposition temperature. When the ACN filler was introduced at 6 wt % into the PLA-based polymeric matrix, the tensile strength of the PLA/ACN-6 nanocomposite was enhanced by 61.3% and the Young's modulus was 1.5-fold greater than those of the neat PLA-F sheet. This was mainly attributed to the endurance of higher stress of the rigid nanocrystals and the interfacial adhesion between filler and matrix. In the meantime, the addition of ACN improved the thermal property of the nanocomposites. Additionally, because of nucleation of the cellulose nanocrystals, the crystalline properties of all nanocomposites were elevated. The superior reinforcing function of ACN derived from natural resources will expand the practical application of PLA-based materials as replacements for traditional petrochemical plastics.

Acknowledgements

The authors are grateful to: the National Natural Science Foundation of China (50843031); 973 Projects of Chinese Ministry of Science and Technology (2007CB936104); Program of Energy Research and Development (PERD) of Canada; Agricultural Bioproducts Innovation Program (ABIP) of Canada via the Pulse Research Network (PURENET); Fundamental Research Funds for the Central Universities (Self-Determined and Innovative Research Funds of WUT 2010-II-022); Youth Chenguang Program of Science & Technology in Wuhan (200850731383); State Key Laboratory of Magnetic Resonance and Atomic and Molecular Physics, Wuhan Institute of Physics and Mathematics, Chinese Academy of Sciences (T152802); State Key Laboratory of Pulp and Paper Engineering, South China University of Technology (200906); and the Key Laboratory of Cellulose and Lignocellulosics Chemistry, Guangzhou Institute of Chemistry, Chinese Academy of Sciences (LCLC-2010-10) for partial funding of this work.

Appendix A. Supplementary data

Supplementary data associated with this article can be found, in the online version, at doi:10.1016/j.carbpol.2010.10.047.

References

Adão, M. H. V. C., Saramago, B. J. V., & Fernandes, A. C. (1999). Estimation of the surface properties of styrene-acrylonitrile random copolymers from contact angle measurements. *Journal of Colloid and Interface Science*, *217*, 94–106.

Attala, R. H., Gast, J. C., Sindorf, D. W., Bartuska, V. J., & Maciel, G. E. (1980). Carbon-13 NMR spectra of cellulose polymorphs. *Journal of the American Chemical Society*, *102*, 3249–3251.

Azizi Samir, M. A. S., Alloin, F., & Dufresne, A. (2005). Review of recent research into cellulosic whiskers, their properties and their application in nanocomposite field. *Biomacromolecules*, *6*, 612–626.

Azizi Samir, M. A. S., Alloin, F., Sanchez, J.-Y., Kissi, N. E., & Dufresne, A. (2004). Preparation of cellulose whiskers reinforced nanocomposites from an organic medium suspension. *Macromolecules*, *37*, 1386–1393.

Azizi Samir, M. A. S., Chazeau, L., Alloin, F., Cavaillé, J.-Y., Dufresne, A., & Sanchez, J.-Y. (2005). POE-based nanocomposite polymer electrolytes reinforced with cellulose whiskers. *Electrochimica Acta*, *50*, 3897–3903.

Bondeson, D., & Oksman, K. (2007). Polylactic acid/cellulose whisker nanocomposites modified by polyvinyl alcohol. *Composites Part A: Applied Science and Manufacturing*, *38*, 2486–2492.

Cao, X., Habibi, Y., & Lucia, L. A. (2009). One-pot polymerization, surface grafting, and processing of waterborne polyurethane-cellulose nanocrystal nanocomposites. *Journal of Materials Chemistry*, *19*, 7137–7145.

Chauve, G, Heux, L., Arouini, R., & Mazeau, K. (2005). Cellulose poly(ethylene-co-vinyl acetate) nanocomposites studied by molecular modeling and mechanical spectroscopy. *Biomacromolecules*, *6*, 2025–2031.

Chazeau, L., Cavaillé, J. Y., & Perez, J. (2000). Plasticized PVC reinforced with cellulose whiskers. II. Plastic behavior. *Journal of Polymer Science Part B: Polymer Physics*, *38*, 383–392.

Chazeau, L., Cavaillé, J. Y., & Terech, P. (1999). Mechanical behaviour above T_g of a plasticised PVC reinforced with cellulose whiskers: A SANS structural study. *Polymer*, *40*, 5333–5344.

Chazeau, L., Paillet, M., & Cavaillé, J. Y. (1999). Plasticized PVC reinforced with cellulose whiskers. I. Linear viscoelastic behavior analyzed through the quasi-point defect theory. *Journal of Polymer Science Part B: Polymer Physics*, *37*, 2151–2164.

Choi, Y., & Simonsen, J. (2006). Cellulose nanocrystal-filled carboxymethyl cellulose nanocomposites. *Journal of Nanoscience and Nanotechnology*, *6*, 633–639.

Dubief, D., Samain, E., & Dufresne, A. (1999). Polysaccharide microcrystals reinforced amorphous poly(β-hydroxyoctanoate) nanocomposite materials. *Macromolecules*, *32*, 5765–5771.

Dufresne, A. (2006). Comparing the mechanical properties of high performances polymer nanocomposites from biological sources. *Journal of Nanoscience and Nanotechnology*, *6*, 322–330.

Dufresne, A. (2008). Polysaccharide nanocrystal reinforced nanocomposites. *Canadian Journal of Chemistry*, *86*, 484–494.

Dufresne, A. (2010). Processing of polymer nanocomposites reinforced with polysaccharide nanocrystals. *Molecules*, *15*, 4111–4128.

Eichhorn, S. J., Dufresne, A., Aranguren, M., Marcovich, N. E., Capadona, J. R., Rowan, S. J., et al., Thielemans, W., Renneckar, S., Veigel, S., Yano, H., Nogi, M., Mangalam, A., Benight, A. S., & Berglund, L. A. (2010). Review: Current international research into cellulose nanofibres and nanocomposites. *Journal of Materials Science*, *45*, 1–33.

Fabbri, P., Champon, G., Castellano, M., Belgacem, M. N., & Gandini, A. (2004). Reactions of cellulose and wood superficial hydroxy groups with organometallic compounds. *Polymer International*, *53*, 7–11.

Favier, V., Canova, G. R., Cavaillé, J. Y., Chanzy, H., Dufresne, A., & Gauthier, C. (1995). Nanocomposites materials from latex and cellulose whiskers. *Polymers for Advanced Technology*, *6*, 351–355.

Garcia de Rodriguez, N. L., Thielemans, W., & Dufresne, A. (2006). Sisal cellulose whiskers reinforced polyvinyl acetate nanocomposites. *Cellulose*, *13*, 261–270.

Grunert, M., & Winter, W. T. (2002). Nanocomposites of cellulose acetate butyrate reinforced with cellulose nanocrystals. *Journal of Polymers and the Environment*, *10*, 27–30.

Habibi, Y., & Dufresne, A. (2008). Highly filled bionanocomposites from functionalized polysaccharide nanocrystals. *Biomacromolecules*, *9*, 1974–1980.

Habibi, Y., Goffin, A.-L., Schiltz, N., Duquesne, E., Dubois, P., & Dufresne, A. (2008). Bionanocomposites based on poly(ε-caprolactone)-grafted cellulose nanocrystals by ring-opening polymerization. *Journal of Materials Chemistry*, *18*, 5002–5010.

Habibi, Y., Lucia, A. L., & Rojas, O. J. (2010). Cellulose nanocrystals: Chemistry, self-assembly, and applications. *Chemical Reviews*, *110*, 3479–3500.

Jiang, L., Morelius, E., Zhang, J., Wolcott, M., & Holbery, J. (2008). Study of the poly(3-hydroxybutyrate-co-3-hydroxyvalerate)/cellulose nanowhisker composites prepared by solution casting and melt processing. *Journal of Composite Materials*, *42*, 2629–2645.

Lin, N., Chen, G., Huang, J., Dufresne, A., & Chang, P. R. (2009). Effects of polymer-grafted natural nanocrystals on the structure and mechanical properties of poly(lactic acid): A case of cellulose whisker-graft-polycaprolactone. *Journal of Applied Polymer Science*, *113*, 3417–3425.

Liu, D., Zhong, T., Chang, P. R., Li, K., & Wu, Q. (2010). Starch composites reinforced by bamboo cellulosic crystals. *Bioresource Technology*, *101*, 2529–2536.

Liu, H., Liu, D., Yao, F., & Wu, Q. (2010). Fabrication and properties of transparent polymethylmethacrylate/cellulose nanocrystals composites. *Bioresource Technology*, *101*, 5685–5692.

Ljungberg, N., Cavaillé, J.-Y., & Heux, L. (2006). Nanocomposites of isotactic polypropylene reinforced with rod-like cellulose whiskers. *Polymer*, *47*, 6285–6292.

Marcovich, N. E., Auad, M. L., Bellesi, N. E., Nutt, S. R., & Aranguren, M. I. (2006). Cellulose micro/nanocrystals reinforced polyurethane. *Journal of Materials Research*, *21*, 870–881.

Martin, O., & Avérous, L. (2001). Poly(lactic acid): Plasticization and properties of biodegradable multiphase systems. *Polymer*, *42*, 6209–6219.

de Menezes, J. A., Siqueira, G., Curvelo, A. A. S., & Dufresne, A. (2009). Extrusion and characterization of functionalized cellulose whiskers reinforced polyethylene nanocomposites. *Polymer*, *50*, 4552–4563.

Michalski, M. C., Hardy, J., & Saramago, B. J. V. (1998). On the surface free energy of PVC/EVA polymer blends: Comparison of different calculation methods. *Journal of Colloid and Interface Science*, *208*, 319–328.

Oksman, K., Mathew, A. P., Bondeson, D., & Kvien, I. (2006). Manufacturing process of cellulose whiskers/polylactic acid nanocomposites. *Composites Science and Technology*, *66*, 2776–2784.

Paralikar, S. A., Simonsen, J., & Lombardi, J. (2008). Poly(vinyl alcohol)/cellulose nanocrystal barrier membranes. *Journal of Membrane Science*, *320*, 248–258.

Petersson, L., Kvien, I., & Oksman, K. (2007). Structure and thermal properties of poly(lactic acid)/cellulose whiskers nanocomposite materials. *Composites Science and Technology*, *67*, 2535–2544.

Petersson, L., Mathew, A. P., & Oksman, K. (2009). Dispersion and properties of cellulose nanowhiskers and layered silicates in cellulose acetate butyrate nanocomposites. *Journal of Applied Polymer Science*, *112*, 2001–2009.

Roohani, M., Habibi, Y., Belgacem, N. M., Ebrahim, G., Karimi, A. N., & Dufresne, A. (2008). Cellulose whiskers reinforced polyvinyl alcohol copolymers nanocomposites. *European Polymer Journal*, *44*, 2489–2498.

Ruiz, M. M., Cavaillé, J. Y., Dufresne, A., Gérard, J. F., & Graillat, C. (2000). Processing and characterization of new thermoset nanocomposites based on cellulose whiskers. *Composite Interfaces*, *7*, 117–131.

Ten, E., Turtle, J., Bahr, D., Jiang, L., & Wolcott, M. (2010). Thermal and mechanical properties of poly(3-hydroxybutyrate-co-3-hydroxyvalerate)/cellulose nanowhiskers composites. *Polymer*, *51*, 2652–2660.

Tolstoguzov, V. (2004). Why are polysaccharides necessary? *Food Hydrocolloids*, *18*, 873–877.

Wang, N., Ding, E., & Cheng, R. (2007). Thermal degradation behaviors of spherical cellulose nanocrystals with sulfate groups. *Polymer*, *48*, 3486–3493.

Wu, Q., Henriksson, M., Liu, X., & Berglund, L. A. (2007). A high strength nanocomposite based on microcrystalline cellulose and polyurethane. *Biomacromolecules*, *8*, 3687–3692.

Xiao, B., Sun, X. F., & Sun, R. C. (2001). Chemical, structural, and thermal characterizations of alkali-soluble lignins and hemicelluloses, and cellulose from maize stems, rye straw, and rice straw. *Polymer Degradation and Stability*, *74*, 307–319.

Zini, E., Scandola, M., & Gatenholm, P. (2003). Heterogeneous acylation of flax fibers. Reaction kinetics and surface properties. *Biomacromolecules*, *4*, 821–827.